

Washington University School of Medicine

Digital Commons@Becker

Open Access Publications

1-14-2021

Hypoxia enhances ILC3 responses through HIF-1 α -dependent mechanism

J L Fachi

L P Pral

J A C Dos Santos

A C Codo

S de Oliveira

See next page for additional authors

Follow this and additional works at: https://digitalcommons.wustl.edu/open_access_pubs


Authors

J L Fachi, L P Pral, J A C Dos Santos, A C Codo, S de Oliveira, J S Felipe, F F F Zambom, N O S Câmara, P M M M Vieira, M Colonna, and M A R Vinolo



ARTICLE OPEN

Hypoxia enhances ILC3 responses through HIF-1 α -dependent mechanism

J. L. Fachi^{1,2}, L. P. Pral¹, J. A. C. dos Santos¹, A. C. Codo³, S. de Oliveira¹, J. S. Felipe¹, F. F. F. Zambom⁴, N. O. S. Câmara^{4,5}, P. M. M. M. Vieira^{3,6,7}, M. Colonna² and M. A. R. Vinolo^{1,6,7} 

Group 3 innate lymphoid cells (ILC3) have a prominent role in the maintenance of intestine mucosa homeostasis. The hypoxia-inducible factor (HIF) is an important modulator of immune cell activation and a key mechanism for cellular adaptation to oxygen deprivation. However, its role on ILC3 is not well known. In this study, we investigated how a hypoxic environment modulates ILC3 response and the subsequent participation of HIF-1 signaling in this process. We found increased proliferation and activation of intestinal ILC3 at low oxygen levels, a response that was phenocopied when HIF-1 α was chemically stabilized and was reversed when HIF-1 was blocked. The increased activation of ILC3 relied on a HIF-1 α -dependent transcriptional program, but not on mTOR-signaling or a switch to glycolysis. HIF-1 α deficiency in ROR γ t compartment resulted in impaired IL-17 and IL-22 production by ILC3 in vivo, which reflected in a lower expression of their target genes in the intestinal epithelium and an increased susceptibility to *Clostridioides difficile* infection. Taken together, our results show that HIF-1 α activation in intestinal ILC3 is relevant for their functions in steady state and infectious conditions.

Mucosal Immunology (2021) 14:828–841; <https://doi.org/10.1038/s41385-020-00371-6>

INTRODUCTION

Oxygen constitutes ~21% of the atmosphere and it is commonly used as substrate for several biochemical reactions.¹ Oxygen is the final electron acceptor in the mitochondrial electron transport chain, which is essential to convert nutrients into intracellular energy and to produce new biomolecules.² However, oxygen can also be converted to several toxic free radicals that can induce modifications in proteins and DNA, damage to cellular organelles and even induce cell death.^{1,2} Hence, it is not a surprise that our cells present a variety of oxygen-sensing mechanisms for regulating its concentrations (i.e., capture, transport, and consumption) and adapt their metabolism and function to fluctuations in O₂ levels.³

In the gastrointestinal (GI) tract, the oxygen tensions change across the length and longitudinally from the tissue in direction to the lumen, in which low levels of oxygen are observed at steady state.^{4,5} Intestinal epithelial cells (IEC) are adapted to this “physiological hypoxia”, which is essential for the proper function of the epithelium.⁵ Intestinal low oxygen availability activates responsive mechanisms in these cells, leading to the expression of genes crucial to the mucosal barrier functionality, such as junctional proteins, antimicrobial peptides, and mucus.^{6,7} Thereby, other cells present in the intestinal mucosa also have to adapt their metabolism and functions according to O₂ fluctuations in the GI tract.

One of the main mechanisms involved on the cellular adaptation to hypoxic environments is hypoxia-inducible factor

(HIF)-1 activation. Expressed in practically all cells of the immune system, as well as in IECs, HIF-1 is a transcription factor composed of 2 subunits, a constitutive subunit called HIF- β and HIF-1 α . The stability of HIF-1 α is regulated through different mechanisms, including at the post-translational level by prolyl-hydroxylases (PHDs).⁸ At normal O₂ levels, iron-dependent PHDs are activated and hydroxylate HIF-1 α , which leads to proteasomal ubiquitination mediated by von Hippel-Lindau tumor suppressor protein.^{8,9} By contrast, in low O₂ levels, PHDs are inactivated, resulting in intracellular accumulation of HIF-1 α , which together with HIF- β and the co-activator p300, translocate to the nucleus, bind to hypoxia-responsive elements, and thus regulate the expression of several genes related to cellular adaptation in the hypoxic environment.^{10–12}

Group 3 innate lymphoid cells (ILC3), which are abundant in the intestinal mucosa, are characterized by expression of the transcription factor ROR γ t and cytokines such as IL-17, IL-22, and GM-CSF.¹³ These cells are known to respond to signals such as IL-1 β and IL-23 released by resident cells following tissue damage¹⁴ and to participate in regulation of the intestinal barrier and host-microbiota interactions.¹⁵ ILC3 also contribute to the response during intestinal infectious conditions, such as those caused by *Citrobacter rodentium* and *Clostridioides difficile*.^{16–18}

In this study, we explored the role of hypoxia and HIF-1 in the ILC3 responses. We demonstrate that hypoxia increased numbers, proliferation and activation of ILC3 through a HIF-1 α -dependent

¹Laboratory of Immunoinflammation, Department of Genetics, Evolution, Microbiology and Immunology, Institute of Biology, University of Campinas, Campinas, Brazil; ²Department of Pathology and Immunology, Washington University School of Medicine, Saint Louis, MO, USA; ³Laboratory of Immunometabolism, Department of Genetics and Evolution, Microbiology and Immunology, Institute of Biology, University of Campinas, Campinas, Brazil; ⁴Renal Division, Department of Clinical Medicine, Faculty of Medicine, University of São Paulo, São Paulo, Brazil; ⁵Department of Immunology, Institute of Biomedical Sciences, University of São Paulo, São Paulo, Brazil; ⁶Experimental Medicine Research Cluster, Campinas, Brazil and ⁷Obesity and Comorbidities Research Center (OCRC), University of Campinas, Campinas, Brazil

Correspondence: M. Colonna (mcolonna@wustl.edu) or M. A. R. Vinolo (mvinolo@unicamp.br)

These authors contributed equally: J. L. Fachi, L. P. Pral

Received: 26 August 2020 Revised: 8 December 2020 Accepted: 8 December 2020

Published online: 14 January 2021

mechanism. Using conditional knockout mice and pharmacological inhibitor, we found that hypoxia-induced ILC3 activation is due to a direct ability of HIF-1 α to modulate the transcriptional state, via expression of ROR γ t and target-genes. This process is independent of HIF-1 α -induced metabolic regulation. Finally, our study indicates that in the absence of HIF-1 α signaling, mice are more susceptible to intestinal infection by *C. difficile*. These results reveal an important role of hypoxia and HIF-1 stabilization in ILC3, which functionally modulate their transcriptional activation and performance in the intestinal lamina propria.

RESULTS

Low oxygen levels are associated with higher ILC3 response

We first tested whether low levels of oxygen are associated with small intestine (si)-ILC3 activation. Cells were incubated for 3 h in hypoxia or normoxia in the presence or not of IL-1 β /IL-23 stimuli and then were analyzed by flow cytometry using the gate strategy described in Fig. 1a and Supplementary Fig. S1.^{19–21} Under hypoxia, IL-1 β /IL-23-stimulated Lin⁺CD45^{low}CD90.2⁺ cells (ILC3-enriched cell population) had higher levels of ROR γ t, IL-22 and IL-17 proteins than normoxic cells (Fig. 1b). In particular, IL-22 and IL-17 were modulated by hypoxia itself, regardless of the stimuli. These results were corroborated by an increase in relative gene expression in the MNK3 ILC3 cell line (Fig. 1c), indicating that low levels of oxygen were associated with greater ILC3 activation. The observed phenotypes were not associated with any effect on MNK3 cell viability, as demonstrated by Annexin-V/7-ADD staining (Fig. 1d). Likewise, in hypoxia, ILC3 proliferation was increased, as demonstrated by higher incorporation of EdU in MNK3 cells and expression of the proliferation marker Ki67 in primary ILC3s (Fig. 1e, f). For hypoxia induction, we used an anaerobic gas generator, which consumes all oxygen within 3 h, similar to Dang et al.²² The results were confirmed in MNK3 cells incubated for the same period with controlled oxygen levels (8% O₂) and compared with cells in normoxia (Supplementary Fig. S2A and S2B).

ILC3 activation in hypoxia is associated with HIF-1 α stabilization
To assess whether the hypoxia-induced effect was dependent on exposure time, cells were incubated for 1 h at hypoxia or normoxia. This time was enough to increase the expression of ROR γ t, IL-22, and IL-17 in MNK3 cells (Supplementary Fig. S2C). Considering the rapid response to oxygen fluctuation, we next evaluated stabilization of HIF-1 α in the MNK3 cell line incubated under normoxia/hypoxia. We observed that cytokine-stimulated cells presented an increase in HIF-1 α levels compared to unstimulated controls in normoxia (Fig. 2a, b). The levels of HIF-1 α were increased in cells incubated in hypoxic atmosphere. This occurred regardless of IL-1 β /IL-23 stimulation (Fig. 2a, b). Additionally, we analyzed by FACS the content of HIF-1 α in ILC3 subsets. NCR⁺ and CCR6⁺ ILC3 subsets expressed comparable levels of HIF-1 α , while NCR⁻ ILC3 showed a small increase in the content of this protein compared to the other subsets (Fig. S2D).

To gain insight into the relevance of HIF-1 in the ILC3 phenotype under low oxygen levels, we tested the effect of its pharmacological activation and inhibition. A potent and selective inhibitor of HIF-1 α (Bay 87–2243) induced a dose-dependent reduction of MNK3 activation in normoxia and hypoxia (Fig. 2c). In contrast, the HIF-1 α prolyl-hydroxylase inhibitor (Bay 85–3934), which stabilizes HIF-1 α even in the presence of oxygen, showed the opposite phenotype in normoxia, as increased Bay 85–3934 concentrations led to increased production of IL-22 and IL-17 by MNK3 cells (Fig. 2d). Under low levels of O₂, we did not observe any additional effect of HIF-1 α stabilization following Bay 85–3934 treatment on expression of genes related to MNK3 activation (Fig. 2e). We further confirmed that HIF-1 was more active in MNK3 cells under hypoxia by incubating with Bay 85–3934 and evaluating the expression of its target genes *Ldha*, *Slc2a1*, *Pfkfb3*, and *Tff3*, which were all increased (Fig. 2f).

Hypoxia-boosted ILC3 activation is independent of mTOR signaling

To gain insight into the mechanisms involved in the activation of ILC3 under hypoxia, we first tested whether ILC3 relies on mammalian target of rapamycin (mTOR) signaling for metabolic adaptation to low oxygen levels. The mTOR pathway is a central regulator of mammalian metabolism and physiology, acting as a protein kinase that regulates complex cellular functions.²³ As already shown,²⁰ rapamycin, a mTOR inhibitor, decreases MNK3 expression of ROR γ t, IL-22, and IL-17 in normoxia, which indicates that mTOR sustains cell-intrinsic activation (Fig. 3a). However, the increased expression of ROR γ t, IL-22, and IL-17 observed during hypoxia was not affected by the presence of rapamycin (Fig. 3a), indicating that ILC3 cell line activation at low oxygen levels is independent of mTOR signaling. Since mTORC1 drives glycolytic metabolism and mTOR is related to HIF-1 α stabilization, we next measured HIF-1 α expression in MNK3 cells incubated with rapamycin in normoxia and hypoxia. Rapamycin reduced HIF-1 α expression in stimulated MNK3 in normoxia, an effect that was absent in cells incubated in hypoxia (Fig. 3b). Similarly, IL-23/IL-1 β -activated MNK3 cells under hypoxia had increased glucose uptake and produced more lactate than cells in normoxia (Fig. 3c, d). Although rapamycin reduced glucose uptake and lactate production in normoxic atmosphere, no effects were observed under hypoxic conditions, which further indicates that ILC3 do not depend on mTOR signaling at low oxygen levels (Fig. 3c, d). Contributing to the hypothesis that hypoxia-boosted ILC3 activation is independent of glycolytic metabolism, inhibition of glycolysis with 2-DG had only a minor effect in MNK3 acute response under hypoxia. Despite the ROR γ t expression, the IL-17 and IL-22 levels were still elevated after 2-DG treatment in hypoxia compared to normoxia (Fig. 3e). Together, these data suggest that boosted activation of ILC3 by hypoxia was independent of glycolysis and mTOR activation.

Hypoxia boosts ILC3 activation independently of mitochondrial fitness

To determine whether oxygen levels modify the cellular energy program, since we investigated the total mitochondrial content of MNK3 cells with MitoTracker Green. Different combinations of IL-23, IL-1 β , rapamycin, and HIF-1 α stabilizer did not affect mitochondrial mass in normoxia and reduced mitochondrial mass under hypoxia. This effect was more evident when cells were treated with rapamycin or HIF-1 α stabilizer (Fig. 3f). We also evaluated the mitochondria function, distinguishing between mitochondria with (respiring) and without (dysfunctional) membrane potential. We observed increased dysfunctional mitochondria load (MitoTracker Red⁺MitoTrackerGreen^{high}) in stimulated-MNK3 cells treated with rapamycin and HIF-1 α stabilizer under normoxia (Fig. 3g). In addition, low oxygen levels potentiated mitochondria dysfunction, even when the mTOR pathway was inhibited. Next, we assessed the metabolic profile of cells with blocked mTORC activity (rapamycin) and increased HIF-1 levels (stabilizer) by real-time analysis of oxygen consumption rate (OCR) at normal oxygen level (Fig. 3h). Unstimulated MNK3 cells had lower maximal respiratory capacity and ATP production than cells stimulated with IL-1 β /IL-23 (Fig. 3h,j), suggesting increased energy demand. However, no difference on OCR was observed in MNK3 cells treated with rapamycin, HIF-1 α stabilizer or combination of both, suggesting a mTORC-independent effect of HIF-1 on ILC3 cell line response. We also observed no differences on basal respiration, non-mitochondrial oxygen consumption, spare respiratory capacity, and acute response by the OCR analysis (Supplementary Fig. S3A–D). The energy map showed higher overall energetic profile instead of a glycolytic dominant profile in stimulated MNK3 compared to resting cells (Supplementary Fig. S3E). Rapamycin and HIF-1 α increased levels did not show major differences compared to stimulated cells (Supplementary Fig. S3E). These data indicate that hypoxia boosts ILC3/MNK3 activation through a HIF-1-dependent mechanism and independently of glycolysis and mitochondrial fitness.



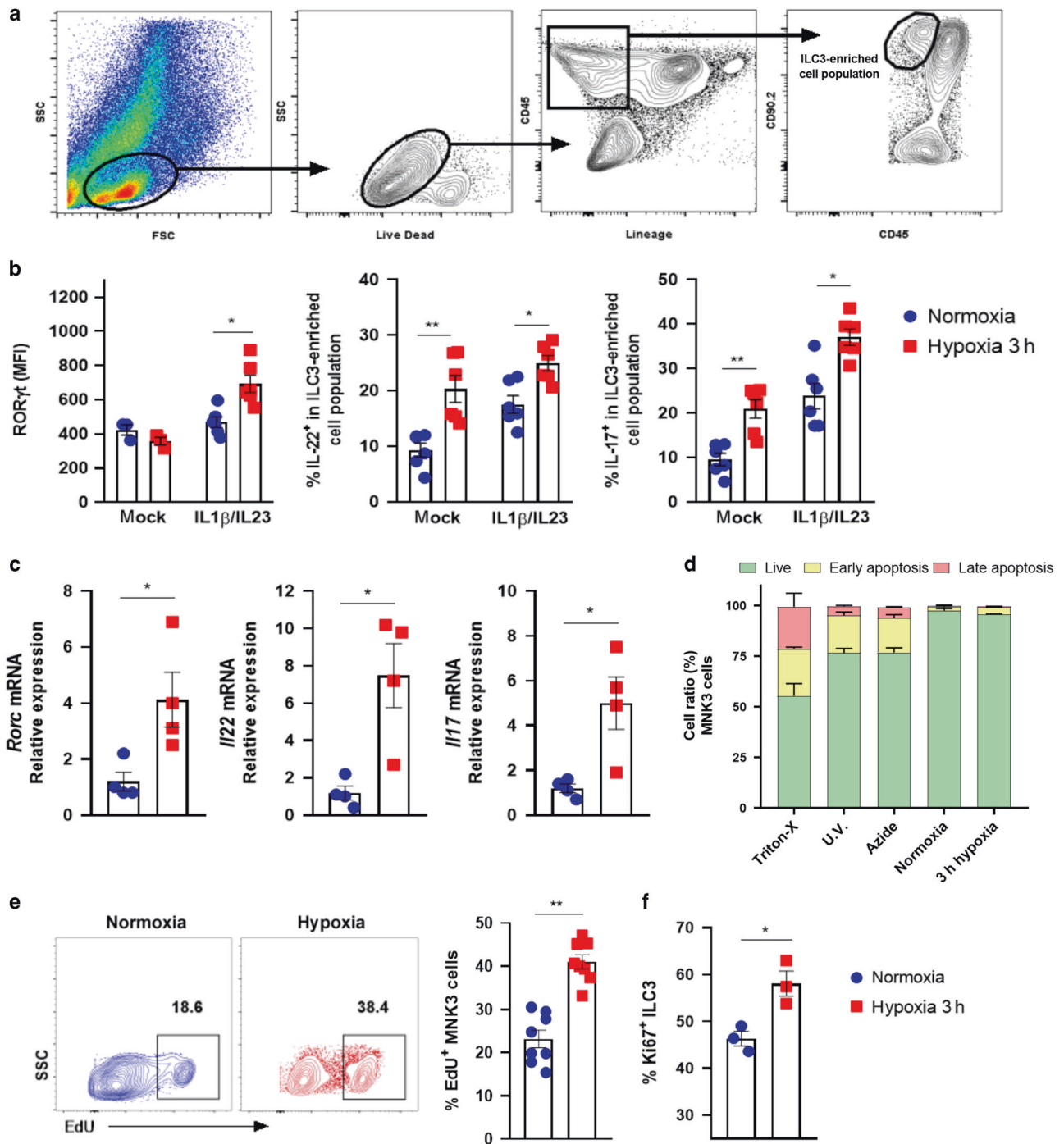


Fig. 1 Hypoxia increases ILC3 activation and proliferation. **A** Gating strategy of live Lin⁺CD45^{low}CD90.2^{high} enriched ILC3 population from small intestine (si) lamina propria (as shown in Fig. S1). **B** ROR γ t mean fluorescence intensity and production of IL-17 and IL-22 by enriched si-ILC3 subset obtained after incubation for 3 h, under normoxia/hypoxia. Cells were non-stimulated (mock) or stimulated with IL-1 β + IL-23 ex vivo ($n = 6$). **C** Relative *Rorc*, *Il22* and *Il17* mRNA expression in stimulated MNK3 cells under normoxia/hypoxia ($n = 4$). **D** Cellular viability of MNK3 cells incubated 3 h in hypoxia/normoxia using annexin-V/7-AAD staining. Live (green) represents the double-negative population, early apoptosis (yellow) shows annexin-V⁺7-AAD⁻, and late apoptosis (red) is double positive cells ($n = 4$). Percentage of EdU⁺ MNK3 cells (**E**) and Ki67⁺ cells in the ILC3-enriched population (**F**) as measured by flow cytometry ($n = 7$ and 3, respectively). Representative EdU⁺ plots are presented on the left. Results are representative of at least two independent experiments and presented as mean \pm SEM. * $p < 0.05$; ** $p < 0.01$.

The transcriptional interaction of HIF-1 α -ROR γ t is crucial for hypoxia-activated ILC3
 Chromatin immunoprecipitation (ChIP) assay was performed for identifying genomic loci that directly or indirectly interact with HIF-1 α in MNK3 cells. As expected, we identified known HIF-1 α target genes that directly bound to HIF-1 α and were upregulated

in hypoxia, such as aldolase (*Aldoa*), lysyl oxidase (*Lox*), and *Serpine1* (Fig. 4a). ROR γ t (*Rorc*) gene also showed approximately eightfold higher interaction with HIF-1 α in hypoxia than normoxia, suggesting that HIF-1 directly regulates *Rorc* expression (Fig. 4b). Similarly, immunoprecipitation was enriched for genes associated with ILC3 function, *Il17* and *Il22*, through the ROR γ t-flanking site

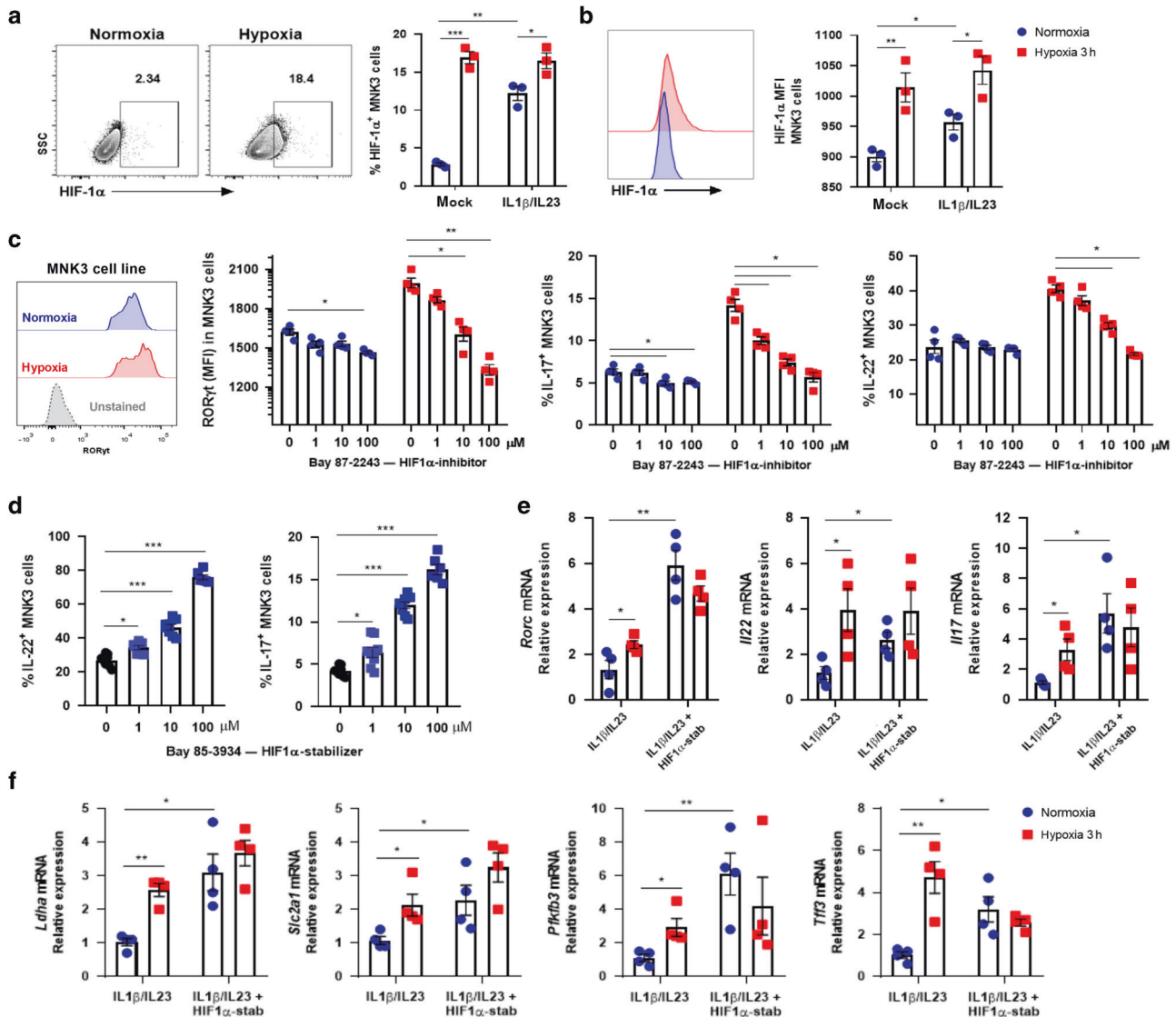


Fig. 2 Hypoxia-induced HIF-1 α stabilization boosts ILC3 cell line activation. HIF-1 α content in MNK3 cells incubated for 3 h under hypoxia/normoxia, as measured by flow cytometry. Graphs indicate **A** percentage of HIF-1 α ⁺ cells and **B** HIF-1 α geometric MFI ($n = 3$). Representative FACS plots on the left. ROR γ t geometric MFI and IL-17 and IL-22 content in stimulated MNK3 cells after 3 h in normoxia/hypoxia with different concentrations of HIF-1 α inhibitor, Bay 87-2243 (inhib) (**C**), or stabilizer, Bay 85-3934 (stab) (**D**) ($n = 4$ and 6, respectively). A representative histogram of ROR γ t expression in MNK3 cells is shown in figure C on the left. Relative mRNA expression of *Rorc*, *Il22*, *Il17* (**E**), and HIF-1 target genes (*Ldha*, *Slc2a1*, *Pfkfb3*, and *Tff3*) (**F**) of MNK3 cells stimulated during 3 h in normoxia/hypoxia and treated or not with HIF-1 α stabilizer ($n = 4$). Results are representative of at least two independent experiments and presented as mean \pm SEM. * $p < 0.05$; ** $p < 0.01$; *** $p < 0.001$.

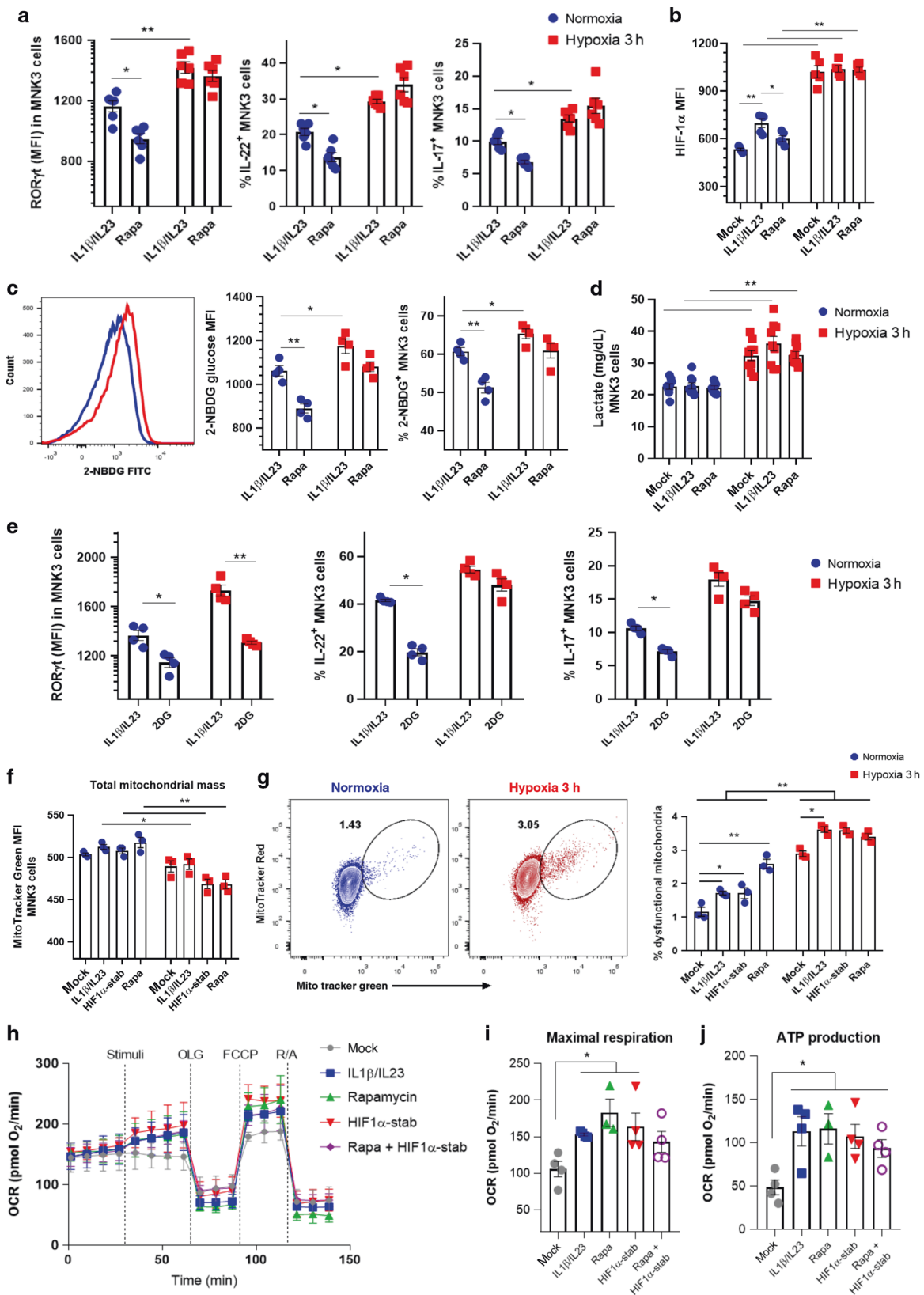
(Fig. 4c, d), indicating that ILC3-related genes are transcriptionally regulated by HIF-1 α under hypoxia.

HIF-1 α deletion results in reduced numbers and less functional ILC3

Next, we used HIF-1 α conditional knockout mice to evaluate the physiological role of this hypoxia-induced transcription factor on ILC3 in ROR γ t expressing cells (Fig. 5a, b). HIF-1 α deficiency in ROR γ t⁺ cells (KO), which included ILC3, was associated with a significant reduction of si-ILC3 number (Fig. 5c, d), and lower expression of ROR γ t and IL-22/IL-17 in ILC3 compared to the control littermates (HIF-1 α ^{flxed} mice, or WT) (Fig. 5e, f). This effect was accompanied by an increase of ILC1 numbers and its T-bet expression and no effect on ILC2 (Fig. 5d, e). ILC3-enriched cell population from HIF-1 α deficient mice, in opposition to cells from HIF-1 α sufficient mice, were not responsive to HIF-1 α stabilizer treatment ex vivo, confirming the hypothesis that HIF-1 is relevant

for the effect of this drug on ILC3 (Fig. 5f). No differences were observed in expression of *Il23r* or *Il1r* in MNK3 cells after 3 h in hypoxia compared to normoxia (Supplementary Fig. S4A) or in HIF-1 α -deficient ILC3 compared to wild-type cells (Supplementary Fig. S4B), indicating that hypoxia-induced HIF-1 α stabilization does not improve ILC3 responsiveness to IL-23 and IL-1 β . Likewise, knocking out HIF-1 α in IEC did not result in quantitative or functional differences in ILCs, particularly ILC3 (Supplementary Fig. S4C–G).

Next, we tested whether mice subjected to a hypoxic condition would show differences in ILC3s activation and some of their targets in the small intestine. HIF-1 α deficient mice (HIF-1 α ^{Δ Rorc} or KO) and littermate controls (HIF-1 α ^{fl/fl} or WT) were maintained in a normobaric chamber at 8% oxygen for 48 h and compared with mice in normoxia (Fig. 6a). Wild-type mice showed an increase of lymphocytes, ILC2 and ILC3 number, as well as reduction of ILC1, in the SI when maintained under hypoxia and compared to



normoxia controls (Fig. 6b). HIF-1 α ^{ΔRorc} mice also presented an increased number of lymphocytes, ILC2 and, although less pronounced, ILC3 in hypoxia compared to normoxia (Fig. 6b). Comparing KO to WT mice, the HIF-1 α absence was associated to

reduced ILC3 and increased ILC1 frequency, regardless of oxygen level (Fig. 6b). This phenotype was accompanied by lower ROR γ t and increased T-bet expression in ILC3 compartment from KO mice (Fig. 6c). No effect was observed on the ILC2 expression of

Fig. 3 ILC3 cell line under hypoxia do not depend on glycolytic metabolism and mitochondrial respiration. **A** ROR γ t geometric MFI and IL-22 and IL-17 content in stimulated MNK3 cells after 3 h under normoxia/hypoxia with and without rapamycin treatment ($n = 6$). **B** HIF-1 α geometric MFI in MNK3 cells incubated 3 h under normoxia or hypoxia with different conditions: unstimulated (mock); IL-1 β and IL-23 stimulated; and IL-1 β , IL-23 and rapamycin (Rapa) treated ($n = 5$). **C** Uptake of glucose (2-NBDG) by flow cytometry in stimulated MNK3 cells with and without rapamycin treatment ($n = 4$). A representative histogram is on the left and graphs showing MFI and percentages are on the right. **D** Lactate release by MNK3 cells during 3 h incubation in hypoxia/normoxia under different conditions, as described in B ($n = 9$). **E** ROR γ t geometric MFI and IL-22 and IL-17 content in stimulated MNK3 cells, treated with 2DG for 3 h under normoxia/hypoxia ($n = 4$). **F** Total mitochondrial mass and mitochondrial membrane potential (**G**) in MNK3 cells labeled with MitoTracker Green and MitoTracker Red after 3 h incubation in normoxia or hypoxia ($n = 3$). Cells were stimulated with IL-1 β + IL-23 and treated or not treated with HIF-1 α stabilizer (stab) or rapamycin. Real-time changes (**H**), maximal respiratory capacity (**I**), and ATP production (**J**) in the OCR of MNK3 cells after stimulation and treatment with oligomycin (OLF), FCCP, and rotenone/antimycin A (R/A) ($n = 4$). Cells were stimulated or not with IL-1 β + IL-23 and treated or not with HIF-1 α stabilizer (stab) and/or rapamycin. Results are performed at least twice (except H-J) and presented as mean \pm SEM. * $p < 0.05$; ** $p < 0.01$.

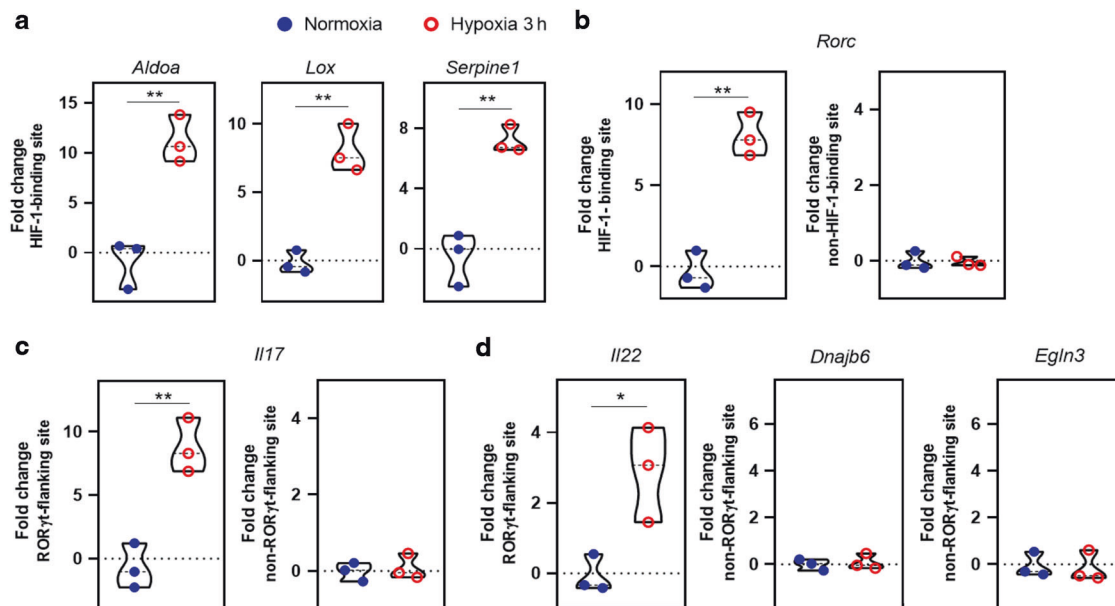


Fig. 4 Hypoxia induces HIF-1 α -ROR γ t interaction and transcriptional fate in ILC3. Analysis of HIF-1 interaction with genes using the chromatin immunoprecipitation (ChIP) technique. MNK3 cells were incubated for 3 h in hypoxia or normoxia without stimulation and then HIF-1 α -associated chromatin sites were purified and amplified by qPCR ($n = 3$). **A** Measurement of HIF-1 α binding to HIF-1 α -responsive genes under hypoxia. **B** Measurement of HIF-1 α binding to known HIF-1-binding or non-binding sites of *Rorc*. **C** Measurement of HIF-1 α binding to the ROR γ t-flanked or not flanked sites of *Il17*. **D** Measurement of HIF-1 α binding to *Il22* and non-ROR γ t-flanking *Dnajb6* and *Egl3* genes. All ChIP-qPCR data were normalized by log₂-fold change of total chromatin extraction (input) to purified immunoprecipitated chromatin. Results are representative of two independent experiments and presented as mean \pm SEM. * $p < 0.05$; ** $p < 0.01$.

Gata3 (Fig. 6c). We also observed increased proliferation of ILC3-enriched population in WT mice under hypoxia, which was reduced in KO, and greater tendency of ILC1 to proliferate in KO mice in both normoxia or hypoxia (Fig. 6d), suggesting a shift on the ILC1/ILC3 ratio at lower O₂ levels or HIF-1 α deficiency. We also found higher expression of IL-22, IL-17, and their target genes in the small intestine of WT mice in hypoxia compared to normoxia (Fig. 6e, f). These effects were attenuated when HIF-1 α was deleted (Fig. 6e, f).

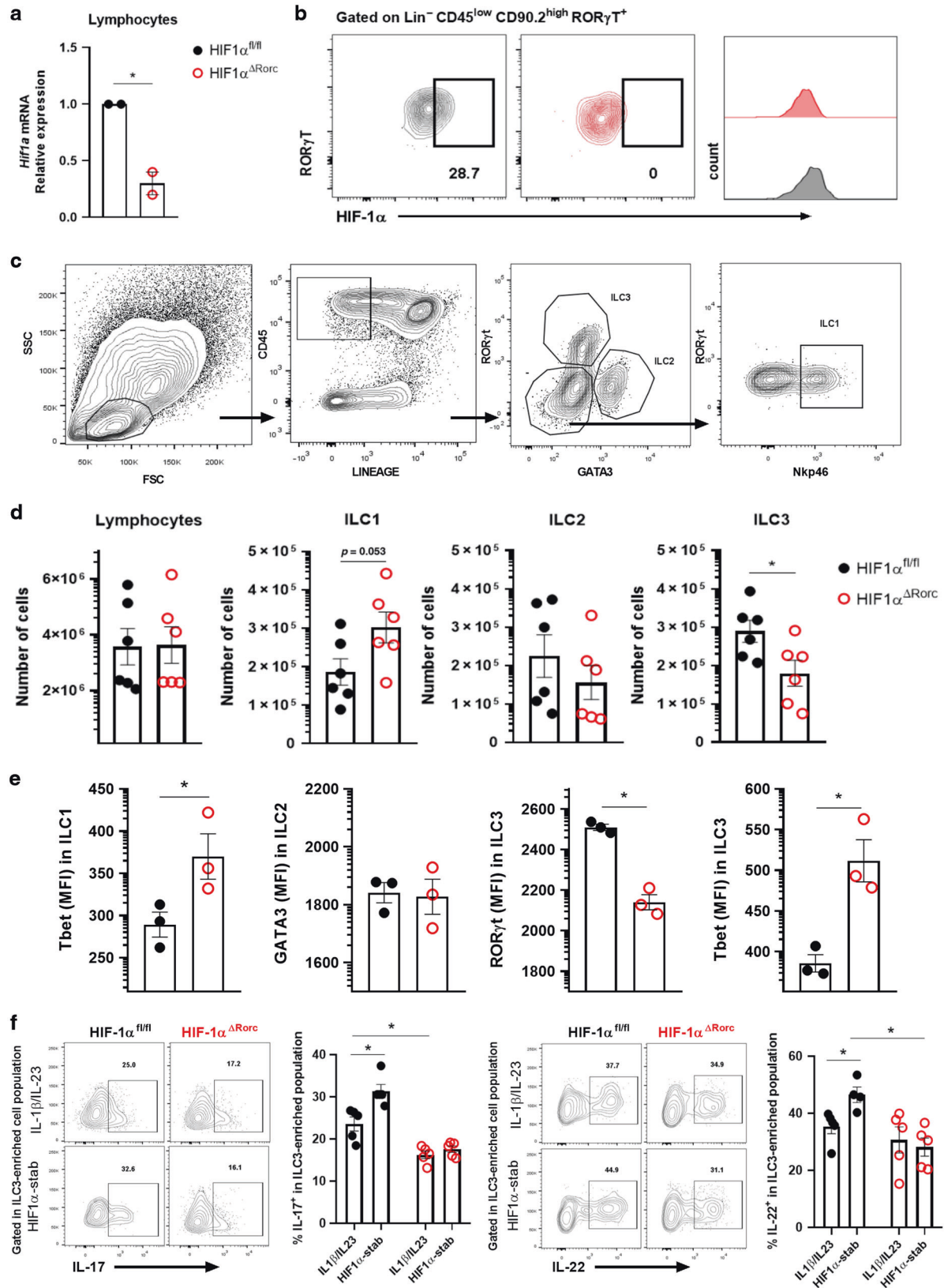
HIF-1 α -deficient *Rorc* mice are more susceptible to *C. difficile* infection

To determine the relevance of HIF-1 α in the role of ILC3 during an inflammatory/infectious condition, we used the *C. difficile* infection (CDI) model, previously shown to have an important role of ILC3 and IL-22.^{17,21,24} We infected HIF-1 α conditional knockout mice with *C. difficile* and assessed the impact of HIF-1 α on ILC3 function during colitis (Fig. 7a). We observed increased susceptibility of KO to CDI compared to WT. KO mice presented higher clinical scores, lost more body weight during infection, and displayed significant reduced size of the colon and small intestine compared to WT (Fig. 7b–d). We also observed high tissue damage and increased translocated bacterial to the liver, spleen and mesenteric lymph

nodes in KO mice, consistent with the reduction in intestinal barrier function and immune response during the acute phase of infection (Fig. 7e, f). Similar to uninfected mice (Fig. 5), we observed a significant reduction in the number of ILC3 and increased ILC1 in the colon and SI of KO compared to WT mice (Fig. 7g, h). HIF-1 α deficient mice also presented several functional changes in the ILC1/ILC3 ratio (Fig. 8). Increased ILC1 proliferation, T-bet content and *Ifng* mRNA expression was observed in infected KO compared to WT mice (Fig. 8a–e). On the other hand, a reduction of ILC3 proliferation and activation was observed in the absence of HIF-1 α in the ROR γ t⁺ compartment (Fig. 8a–e). These findings were accompanied by a downregulation of IL-22 and IL-17 target genes expression in the colon of infected HIF-1 α -deficient mice (Fig. 8f), suggesting that ILC3 activation by HIF-1 signaling has a crucial role in maintaining the intestinal mucosal barrier and is a key component for mucosal immune response during intestinal *C. difficile* infection (Supplementary Fig. S5).

DISCUSSION

We demonstrated that low oxygen levels boost intestinal ILC3 activation and proliferation. The observed phenotype was lost by deleting or chemically inhibiting HIF-1 α stabilization, showing that



functional ILC3 responses to hypoxia lean towards HIF-1 signaling. Previous studies have shown participation of HIF-1 in functional control of different immune cell subsets.²⁵ Hypoxia-induced HIF-1 activation improves differentiation, proliferation and metabolic

reprogramming of Th17 and Treg cells.^{22,26–28} The antitumor capacity of CD8 T cells is also increased by HIF-1 via induction of glycolytic metabolism, tumor infiltration and tumoricidal memory formation.^{29,30} Likewise, recent studies have shown participation

Fig. 5 HIF-1 $\alpha^{\Delta Rorc}$ mice have lower number and less functional ILC3 at steady state. Relative *Hif1a* mRNA expression in total lymphocytes (A) and FACS plots of HIF-1 α content in Lin⁺CD45^{low}CD90.2^{high}ROR γ t⁺ ILC3 (B) from HIF-1 $\alpha^{\Delta Rorc}$ and HIF-1 α^{floxed} small intestine lamina propria. Cells were incubated for 2 h in hypoxia (n = 2). C Gating strategy to identify and quantify ILC subsets in intestinal lamina propria. D Absolute number of ILC subsets in HIF-1 $\alpha^{\Delta Rorc}$ and HIF-1 α^{floxed} small intestine lamina propria (n = 5–6). ILC1, ILC2 and ILC3 are defined as Lin⁺CD45⁺ROR γ t⁺Gata3⁺Nkp46⁺, Lin⁺CD45⁺ROR γ t⁺Gata3⁺ and Lin⁺CD45⁺ROR γ t⁺Gata3⁻, respectively. Lineage was defined by CD3, CD5, CD19, CD11b, and CD11c markers. E Geometric mean fluorescence intensity of T-bet in ILC1, Gata3 in ILC2, and T-bet and ROR γ t in ILC3 from small intestine lamina propria of HIF-1 $\alpha^{\Delta Rorc}$ and HIF-1 α^{floxed} mice (n = 3). F Percentage of IL-17 and IL-22 producing Lin⁺CD45^{low}CD90.2⁺ (ILC3-enriched population) cells from HIF-1 $\alpha^{\Delta Rorc}$ and HIF-1 α^{floxed} mice. Representative FACS plots are presented on the left. Cells were stimulated with IL-1 β + IL-23 ex vivo and treated or not with the HIF-1 α stabilizer (stab) (n = 5). All mice were littermates and matched by sex and age. Results are representative of at least two independent experiments and presented as mean \pm SEM. *p < 0.05.

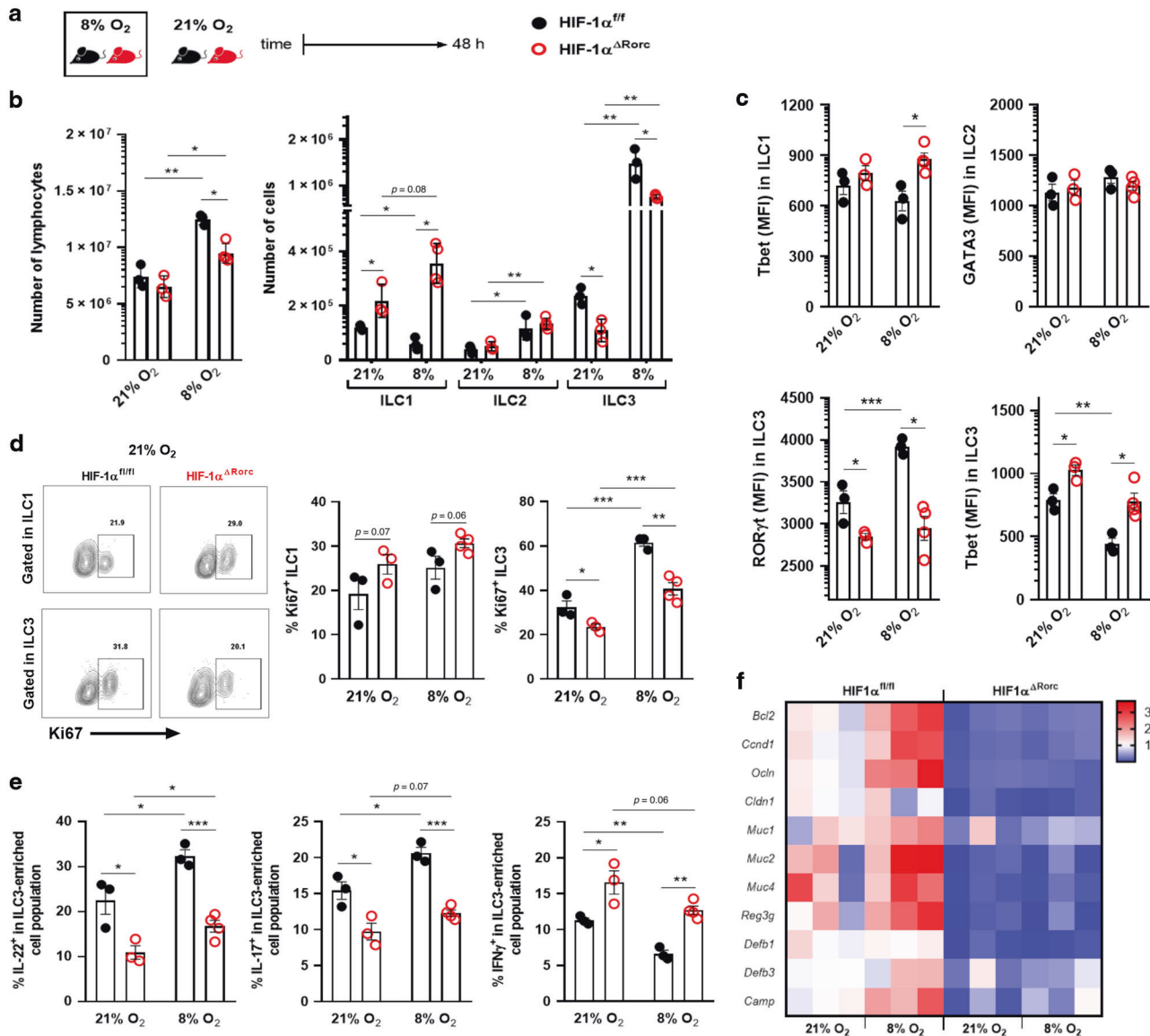
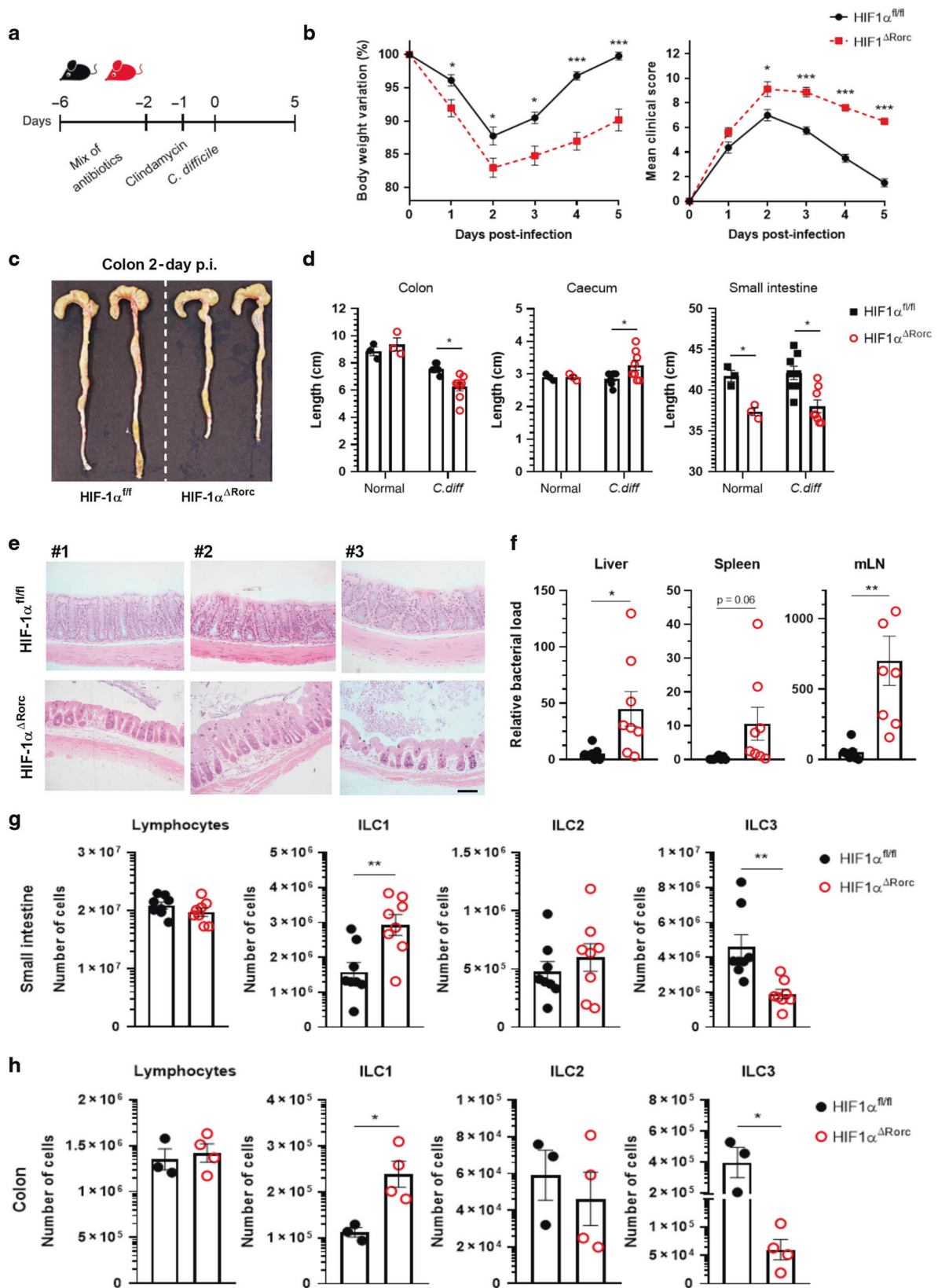


Fig. 6 Acute hypoxia exposure delays ILC3 responses in a HIF-1 manner. A Experimental scheme of HIF-1 $\alpha^{\Delta Rorc}$ and HIF-1 α^{floxed} mice housed under normoxia or 8% O₂-hypoxia, using a normobaric gas chamber, for 48 h. B Absolute number of ILC subtypes in small intestine lamina propria (n = 3–4). ILC1, ILC2, and ILC3 are defined as Lin⁺CD45⁺ROR γ t⁺Gata3⁺Nkp46⁺, Lin⁺CD45⁺ROR γ t⁺Gata3⁺ and Lin⁺CD45⁺ROR γ t⁺Gata3⁻, respectively. C Geometric MFI of T-bet in ILC1, Gata3 in ILC2, T-bet and ROR γ t in ILC3 from si-lamina propria of HIF-1 $\alpha^{\Delta Rorc}$ and HIF-1 α^{floxed} mice kept in normoxia or hypoxia (n = 3–4). D Percentage of Ki67⁺ ILC1 (Lin⁺Tbet⁺, left) and ILC3 (Lin⁺ROR γ t⁺, right) under normoxia or hypoxia (n = 3–4). Representative FACS plots are presented on the left. E Percentage of IL-22, IL-17, and IFN γ producing Lin⁺CD45^{low}CD90.2⁺ (si-ILC3-enriched population) cells from HIF-1 $\alpha^{\Delta Rorc}$ and HIF-1 α^{floxed} mice in normoxia or hypoxia (n = 3–4). F Relative IL-22-target gene expression in distal ileum under normoxia or hypoxia (n = 4). All HIF-1 $\alpha^{\Delta Rorc}$ and HIF-1 α^{floxed} mice were littermates and matched by sex and age. Results are presented as mean \pm SEM. *p < 0.05; **p < 0.01; ***p < 0.001.



of HIF-1 in the innate lymphoid compartment. Tumor-infiltrated NK cells operate under hypoxia and rely on HIF-1 to cytokine production and tumor cell death induction.³¹ HIF-1 activation also directly affects late ILC2 maturation through the IL33-ST2 signaling

pathway.³² Together, our results and published reports highlight the relevance of the HIF-1 pathway for steady state immune system functions in intestinal mucosa and lymphoid tissue, and in tumoral, ischemic and inflamed environments.

Fig. 7 HIF-1 $\alpha^{\Delta Rorc}$ mice are more susceptible to *C. difficile* infection. **A** Scheme of *C. difficile* infection model. HIF-1 $\alpha^{\Delta Rorc}$ and HIF-1 α^{floxed} received a mixture of antibiotics for 4 days and then received a single i.p. dose of clindamycin. Mice were then infected with 10^8 CFU of *C. difficile*. **B** Body weight changes and clinical score during *C. difficile* infection ($n = 8$). Image of colons (**C**) and lengths (**D**) of colon, cecum and small intestine from *C. difficile*-infected mice on day 5 ($n = 3-8$). **E** Representative histological sections of colons stained with hematoxylin and eosin from *C. difficile*-infected mice on day 5 ($n = 4$). Scale bar represents 100 μm . **F** Bacterial translocation into the mesenteric lymph nodes (mLN), spleen and liver assessed by qPCR at day 5 ($n = 7-8$). Absolute number of Lin⁺CD45⁺ ILC subtypes in small intestine (**G**) or colon (**H**) lamina propria from infected mice on day 5 ($n = 3-8$). All HIF-1 $\alpha^{\Delta Rorc}$ and HIF-1 α^{floxed} mice were littermates and matched by sex and age. Results are pools of two independent experiments and presented as mean \pm SEM. * $p < 0.05$.

Massive cellular activities require energy-generating precursors for lipid, nucleotide and amino acid synthesis, necessary for an effective response, such as proliferation and gene expression. Naive T cells use oxidative phosphorylation as the main source of energy, different from activated T cells, that shifts to aerobic glycolysis and glutamine catabolism for energy production and biosynthetic precursors.^{33,34} Th17 development is improved by the mTOR-HIF-1 α axis, which controls transcriptional activation of ROR γ t and sustains glycolysis.^{22,28} The mTORC1-HIF-1 α axis also sustains ILC3 responses toward glycolysis and ROR γ t expression in normoxia.²⁰ Although ILC3 and Th17 overlap, ILC3 activation increases mitochondrial respiration and its production of reactive oxygen species (mROS), that stabilizes HIF-1 α under normoxia and inhibits pyruvate dehydrogenase kinase, in contrast to Th17.^{20,35} However, our work showed that activation of ILC3 in hypoxia does not depend on glycolysis or mitochondrial respiration. Similarly, Velasquez *et al.* showed that IL-15-stimulated NK cells were more activated under acute hypoxia, with increased glycolytic gene expression without major changes in glycolytic flux or glucose consumption.³⁶ In addition, HIF-1 disrupts the pattern of genes expressed by cells enabling it to interact with other transcription factors and regulate their stability or activity. This has already been demonstrated for ROR γ t and Foxp3 in T helper cells.²² Thus, here we showed that HIF-1 activation in hypoxia boosts ILC3 activation through its transcriptional ability to increase the ROR γ t expression and activity. Further investigation will be necessary to validate the molecular HIF-1-ROR γ t interaction.

We have also observed a crucial role in hypoxia-induced HIF-1 α activation for maintaining intestinal mucosa and increasing resistance to *C. difficile* infection. Healthy intestinal microbiota brings mutual benefits and assists in resistance to colonization by pathogens. However, due to the use of antibiotics and microbiota imbalance, *C. difficile* proliferates and produces toxins, causing inflammation in colon mucosa, which ranges from benign to fulminant colitis.³⁷ Microbiota contributes to low oxygen content in the intestinal lumen, which is relevant for its host interactions along the whole intestinal tract.^{38,39} HIF-1 α stabilization in IECs functionally ensures barrier integrity and colitis protection.^{6,7} Colitis-induced intestinal epithelium disruption causes exposure of luminal bacteria and excessive innate inflammatory responses, related to tumor or lethal colitis development.⁴⁰ We found that intestinal oxygen levels can act on ILC3 activation, inducing increased ILC3 target-gene expression in the epithelium, which is important to maintain the barrier homeostasis. Deletion of HIF-1 in ILC3s compartment impaired the epithelial barrier and the mechanisms controlling bacterial translocation, showing relevance of HIF-1 in the ILC3 role. A previous study showed that deletion of HIF-1 in T cells also affected host protection in DSS-induced colitis and increased cellular infiltration,⁴¹ highlighting the relevance of HIF-1 expression and stabilization in immune cell types, and the epithelium.

Likewise, we found that mice exposed to acute hypoxia at 8% oxygen had a significant functional influence on activation of intestinal ILC3 through subsequent HIF-1 signaling. Low oxygen levels boosted ILC3 activation and cytokine release, impacting on tissue gene expression and mucosal homeostasis. This may have important implications for individuals regularly exposed to drastic changes in the oxygen pressures, such as long-haul flights and differences in sea level (21% O₂) and mountain locations, where

oxygen availability drops dramatically (~11% O₂).¹¹ We also observed an interesting effect of hypoxia and HIF-1 on the ILC1/ILC3 balance in the intestine. As ILC3 expresses ROR γ t and resembles Th17 cells, ILC1 (including NK cells) expresses the transcription factor T-bet and secretes mainly IFN- γ , similar to Th1 responses.¹³ We found that hypoxia-induced HIF-1 signaling increases ROR γ t expression and IL-22/IL-17 production and reduces T-bet and IFN- γ . Consistently, we noticed greater accumulation of ILC1 in the lamina propria, and enhanced expression of T-bet and IFN- γ in HIF-1 α knockout mice. Recent work indicates the presence of several subsets of ILC3 and high plasticity between these populations and other populations of ILCs.⁴² Emerging ROR γ t+ILC3 acquires T-bet expression for subsequent expression of NRC, showing an ILC1-like phenotype and production of TNF, IFN- γ , and IL-22 with lower IL-17.⁴³⁻⁴⁵ Thus, we speculate that HIF-1 α may guarantee the intact ROR γ t-ILC3 profile and minimize their plastic capacity to the ILC1-like phenotype. This aspect and others, such as the role of hypoxia and HIF-1 in the intestinal lymphoid tissue formation, their effects on replacement and migration of ILCs into the intestine and their specific effects on ILC3 subsets will need to be addressed in future studies.

Herein, we highlighted the relevance of hypoxia-induced HIF-1 α stabilization in ILC3 and its consequence to other cells in the intestinal mucosa, such as ILC1 and IECs. Our findings also indicate new therapeutic possibilities, such as drugs that regulate HIF-1 α stability, which could be applied to patients with chronic intestinal inflammation or enteric infections.

METHODS

Mice

Adult C57BL/6 male mice were purchased from the Multi-disciplinary Centre for Biological Investigation, Campinas-SP, Brazil. Rorc-Cre, Villin-Cre, and HIF-1 $\alpha^{floxed/floxed}$ mice were from The Jackson Laboratories. All strains were maintained in a C57BL/6 background and kept in regular filter-top cages with free access to sterile water and food. Animal procedures were approved by the Ethics Committee on Animal Use of the University of Campinas (protocol #5495-1/2020).

Intestinal innate lymphoid cell isolation

Small intestinal or colon samples were harvested, and mesenteric adipose tissue and Peyer's patches removed by dissection before cutting longitudinally and washing out the contents. Intraepithelial lymphocytes were excluded by two 20 min extraction washes with 5 mM EDTA. Intestinal lamina propria immune cells were isolated by digestion with 1 mg/mL collagenase IV (Sigma) for 40 min at 37 °C and shaking. Lymphocytes were enriched over a Percoll gradient (GE Healthcare) (40%/70% interface). Cells were washed, counted in Neubauer's chamber and stimulated *ex vivo* and/or labeled with monoclonal antibodies for analysis by flow cytometry (Table S1).

Cell culture

The MNK3 cell line was previously described as an *in vitro* system to study ILC3 functionality.⁴⁶ MNK3 cells or single-cell preparations of small intestine lamina propria were cultured in complete RPMI



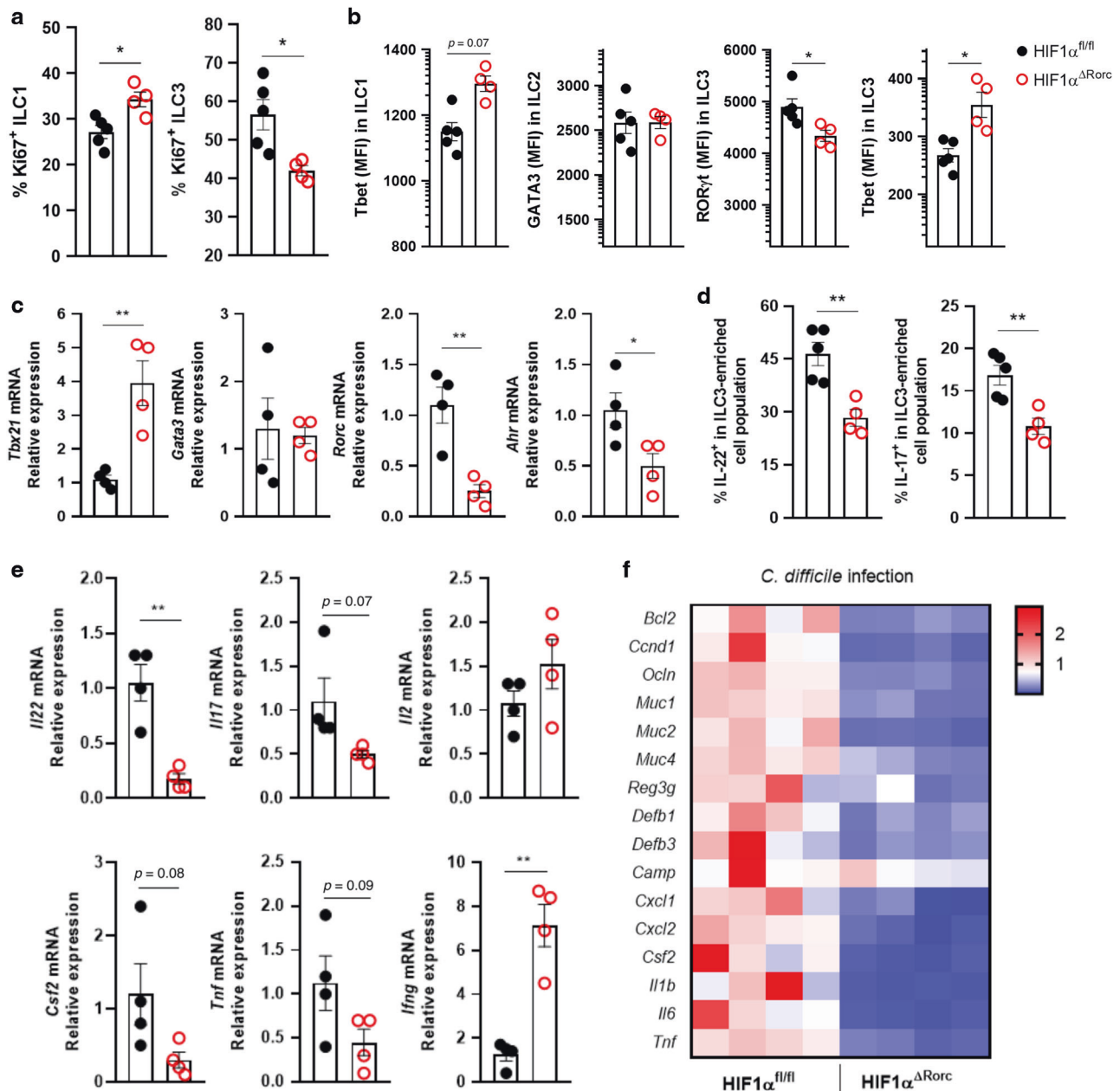


Fig. 8 HIF-1 $\alpha^{\Delta Rorc}$ infected mice have impaired ILC3. **A** Percentage of Ki67⁺ ILC1 (left) and ILC3 (right) from HIF-1 α^{floxed} and HIF-1 $\alpha^{\Delta Rorc}$ infected mice on day 5 ($n = 4-5$). **B** Geometric MFI of Tbet expression in ILC1, Gata3 in ILC2, and Tbet and ROR γ t in ILC3 from small intestine lamina propria of *C. difficile* infected mice on day 5 p.i. ($n = 4-5$). **C** Relative *Tbx21*, *Gata3*, *Rorc*, *Ahr* mRNA expression in total lymphocytes from small intestine lamina propria of infected mice on day 5 ($n = 4$). **D** IL-22 and IL-17 producing Lin⁺CD45^{low}CD90.2⁺ (si-ILC3-enriched population) cells from infected HIF-1 $\alpha^{\Delta Rorc}$ and HIF-1 α^{floxed} mice on day 5 p.i. Cells were stimulated ex vivo with IL-1 β and IL-23 for 3 h ($n = 4$). **E** Relative cytokine mRNA expression in total lymphocytes from small intestine lamina propria of infected mice on day 5 p.i. ($n = 4$). **F** Relative IL-22 and IL-17-target gene expression in the proximal colon of HIF-1 $\alpha^{\Delta Rorc}$ and HIF-1 α^{floxed} mice on day 5 p.i. ($n = 4$). All HIF-1 $\alpha^{\Delta Rorc}$ and HIF-1 α^{floxed} mice were littermates and matched by sex and age. Results are representative of two independent experiments and presented as mean \pm SEM. * $p < 0.05$; ** $p < 0.01$.

(Corning), containing 10% fetal bovine serum, 2 mM GlutaMAX, 1 mM sodium pyruvate, 55 μ M 2-mercaptoethanol, 50 μ g/mL gentamicin and 10 mM HEPES (ThermoFisher). Conditioned medium containing IL-2 and IL-7 was also used to maintain cells. For hypoxia assays, 2×10^5 cells were cultured in polystyrene plates in 96 round-bottomed wells (Corning). Plates were placed into a horizontal sealed jar with an anaerobic gas generator (AnaeroGen, Oxoid; ThermoFisher Scientific), which reduces the oxygen level to $<1\%$ within 3 h. Cells were kept in hypoxic atmosphere for 3 h at 37 $^{\circ}$ C and viability was assessed using the

FITC Annexin V Apoptosis Detection Kit (BD Bioscience). Normoxic controls were incubated during the same period under 21% O₂ and 5% CO₂ at 37 $^{\circ}$ C. Additional experiments were performed under controlled 8% O₂ levels. Cells were in the Cytation 5 Multi-Mode Reader equipped with a Gas controller (BioTek Instruments). For in vitro assays, cells were cultured in complete RPMI with or without a combination of IL-1 β (10 ng/mL) and IL-23 (10 ng/mL) in the presence or absence of Bay 87-2243/HIF-1 inhibitor (1–100 μ M, Sigma-Aldrich), Bay 85-3934/HIF-1 α stabilizer (1–100 μ M, Sigma-Aldrich), rapamycin (20 nM; Millipore), deoxyglucose (2DG,

1 mM, Sigma-Aldrich) and brefeldin A (1:1000, BD Golgi Plug), for 3 h under hypoxia or normoxia.

Flow cytometry

To identify ILC populations, dead single-cell preparations of small intestine or colon lamina propria were excluded using a live/dead cell viability assay in Brilliant Violet 510. A lineage cocktail containing R-phycoerythrin-conjugated monoclonal antibodies against CD3, CD5, CD19, CD11c, and CD11b was used except where stated and population were identified as Lin⁻ and CD45⁺ (PE-Cy7), as already reported^{19–21} (Supplementary Fig. S1B). Surface staining was performed with antibodies diluted in FACS-buffer at 4 °C for 20 min in the dark after blockade of Fc receptors with purified anti-CD16/CD32 (Biolegend). Cells were fixed and intracellularly stained using the Foxp3 Staining Buffer Set (eBioscience) according to manufactures instructions, using monoclonal antibodies to ROR γ t (Percp-Cy5.5), Gata3 (FITC), and T-bet (APC). For functional experiments, MNK3 and small intestine lamina propria (si-LP) cells were cultured in 96-well plates in complete media and stimulated in the presence of Golgi Plug (BD Bioscience) for 3 h at 37 °C. Following incubation, cells were stained for viability and surface molecules, fixed with 2% paraformaldehyde (PFA) and intracellular staining performed using BD Biosciences Fixation/Permeabilization Solution Kit or eBioscience Transcription Factor staining Kit for cytoplasmic or nuclear proteins, such as cytokines and transcription factors (Supplementary Table S1). The ILC3-enriched cell population was identified as Live⁺ Lin⁻ (CD3⁻CD5⁻CD19⁻CD11b⁻CD11c⁻)CD45^{low}CD90.2^{high} (Supplementary Fig. S1A), as already reported.^{19–21} For the proliferation assay, cells were incubated in complete RPMI with EdU or DMSO (20 μ M, Thermo-Fisher Scientific, MA, USA) for 3 h at 37 °C, under hypoxia/normoxia. Following incubation, cells were fixed in 4% PFA and permeabilized with PBS containing 0.05% triton X-100. Detection of EdU-DNA was performed using the Click-iT[™] EdU Cell Proliferation Kit, Alexa Fluor[™] 647 dye (Thermo-Fisher Scientific). Ki67 was stained with a monoclonal antibody after fixing/permeabilizing in vitro cultured cells. For glucose uptake, using 2-deoxy-2-[(7-nitro-2,1,3-benzoxadiazol-4-yl)amino]-D-glucose (2-NBDG, 10 μ g/mL; Invitrogen), cells were incubated in RPMI medium for 2 h at 37 °C under normoxia and hypoxia and measured by flow cytometry. Samples were analyzed on BD FACS-Verse[™] (BD Biosciences) using BD FACSuite[™] Software (BD biosciences). All FACS data were analyzed using FlowJo v.9.5.2 software (Tree Star).

Quantitative gene expression

Total RNA was extracted from tissue using the PureLink[™] RNA kit (Ambion). RNA was converted to cDNA using the High-Capacity cDNA Reverse Transcription Kit (Applied Biosystems) and qPCR was performed using Power SYBR Green PCR Master Mix (Applied Biosystems) and primers indicated in Supplementary Table S2. Quantification of gene expression was performed using 2 ^{$\Delta\Delta$ Ct} method with β 2-microglobulin as a reference gene.

Hypoxia chamber

For acute hypoxic exposures, mice were housed in a normobaric gas chamber (Biospherix, Parish, NY) with circadian cycle/air humidity control, containing continuous electronic nitrogen injection. Oxygen concentrations were maintained at 8–9%, as described by Rempel et al.⁴⁷ After 48 h, mice under hypoxia and their littermate controls under normoxia (21% O₂) were euthanized and tissues harvested to analyze the ILC3 activation.

C. difficile infection

The *C. difficile* VPI 10463 strain was cultivated in BHI blood agar supplemented with hemin (5 μ g/mL) and menadione (1 μ g/mL) at 37 °C in anaerobic atmosphere (AnaeroGen, Oxoid; ThermoFisher Scientific) in jars. 8–10-wk-old age- and gender-matched mice were infected as previously described.⁴⁸ Mice were pre-treated

with antibiotic mixture (0.4 mg/mL kanamycin, 0.035 mg/mL gentamicin, 0.035 mg/mL colistin, 0.215 mg/mL metronidazole, and 0.045 mg/mL vancomycin; Sigma) added to drinking water for 4 days. Next, antibiotics were discontinued and mice received an intraperitoneal single dose of clindamycin (10 mg/kg) (Sigma). After 1 day, mice were infected with 1 \times 10⁸ colony forming units (CFUs) *C. difficile* by gavage. Mice were weighed and monitored daily for clinical severity scores that varied from 0 (normal) to 15 (dead) (Supplementary Table S3).

Histological analysis

Mouse colons were harvested, opened longitudinally and fixed in 4% formalin/0.1% glutaraldehyde. Tissues were processed into histo-resin and 5- μ m sections prepared for staining with Hematoxylin and Eosin solution. Slides were photographed and analyzed using a U-LH100HG Olympus Microscope with 20 \times objective lens.

Bacterial translocation

Spleen, liver and mesenteric lymph nodes were harvested on day 5 of *C. difficile* infection. Bacterial 16S rDNA was extracted using the PureLink[™] Microbiome DNA Purification kit (ThermoFisher Scientific) and gene levels were quantified by qPCR using primers complementary to Eubacteria 16S rDNA conserved region (Supplementary Table S2). Bacterial load was determined using an *E. coli* genomic DNA standard curve and the CFU/g tissue was normalized (gene levels/sample weight).

Lactate measurement

MNK3 cells were cultured in 96-well plates at 2 \times 10⁵ cells per well in complete RPMI medium under hypoxic or normoxic atmosphere for 3 h. Cells were stimulated or not with a combination of IL-1 β (10 ng/mL), IL-23 (10 ng/mL) and rapamycin (20 nM). Following incubation, the supernatant was collected and used for measurement of lactate release with an Enzymatic Lactate Kit, according to manufacturer's instructions (Labtest, MG—Brazil). The absorbance was read at 530 nm and lactate concentrations (mg/dL) determined using a standard control provided in the kit.

Mitochondrial mass

MNK3 cells were seeded in triplicate in 96-wells plate at 2 \times 10⁵ cells/well in complete RPMI (containing 4% IL7 and 2% IL2) and cultured under hypoxic/normoxic atmosphere for 3 h at 37 °C. MitoTracker Green (for total mitochondrial mass) and MitoTracker Red (for mitochondrial membrane potential) staining were performed according to manufacturer's instructions (Invitrogen). Dysfunctional mitochondria were measured as described.⁴⁹ Data were acquired with BD FACS-Verse[™] flow cytometer (BD Biosciences) and analyzed with FlowJo software (Tree Star).

Seahorse metabolic analysis

Real-time analysis of extracellular acidification rate (ECAR) and OCR was performed using an XFe24 Analyzer (Seahorse Bioscience). MNK3 cells were seeded 2 h in quadruplicate at 1 \times 10⁶ cells per well on a pretreated poly-D-lysine-coated 24-well Seahorse plate in complete RPMI containing 4% IL7 and 2% IL2. Cells were washed and cultured in Seahorse Assay Medium containing 10 mM glucose and 1 mM sodium pyruvate for 2 h at 37 °C without CO₂. Oligomycin (ATPase inhibitor, 1 μ M), FCCP (uncoupler of mitochondrial oxidative phosphorylation, 1 μ M), rotenone (complex I inhibitor, 1 μ M) and antimycin A (complex III inhibitor, 1 μ M) were injected where indicated and the ECAR (mpH/min) and OCR (pmol O₂/min) were measured in real time.

Chromatin immunoprecipitation (ChIP)

MNK3 cells were cultured in 12-well plates at 2 \times 10⁶ cells/well in complete RPMI medium under hypoxic or normoxic atmosphere for 3 h at 37 °C. Subsequently, cells were fixed in 1% formaldehyde in PBS for 10 min, quenched with 0.1 M glycine



and processed for ChIP using the MAGnify™ Chromatin Immunoprecipitation System (Invitrogen), following the manufacturer's instructions. ChIP reactions were performed using 3 μ g anti-HIF-1 α antibody/sample (Supplementary Table S1). Protein-s complexes were reverse crosslinked at 65 °C overnight and digested with proteinase K (0.2 μ g/ μ L) for 1 hour at 55 °C. Samples were purified using the Qiagen DNA Purification Kit according to the manufacturer's instructions. Purified DNA was used for qPCR analysis. Input samples (total chromatin extraction, before immunoprecipitation) were analyzed in parallel and used to calculate enrichment in the precipitate by log₂-fold change. Primer sequences are listed in Supplementary Table S2.

Statistical analysis

Analyses were performed using GraphPad software 8.0 (San Diego, CA, USA). All data are presented as mean \pm SEM. All experiments were repeated at least twice, except the Seahorse and hypoxic chamber in vivo exposure assays. Differences were considered significant for $p < 0.05$. Results were compared by Student's t test or Mann Whitney test, as appropriate. For more than two groups, differences were compared by one-way analysis of variance (ANOVA) followed by Tukey's post hoc test.

ACKNOWLEDGEMENTS

This study was supported by research grant from Fundação de Amparo à Pesquisa do Estado de São Paulo (FAPESP, 15/15626–8, 17/16280–3, 18/15313–8, 19/06372–3, and 19/05947–2). The study was also financed by the National Council for Scientific and Technological Development (CNPq) and Coordenação de Aperfeiçoamento de Pessoal de Nível Superior - Brasil (CAPES)—Finance Code 001. J.L.F., L.P.P., A.C.C., and S.O. are recipients of fellowships from FAPESP (2017/06577–9, 2018/02208–1, 2018/22505–0, and 2019/11662–0, respectively). M.C. was supported by MIST (U01 AI095542). We thank Dr. M.A. Portovedo for helping with the ChIP assay.

AUTHOR CONTRIBUTIONS

J.L.F., L.P.P., M.C., and M.A.R.V. provided substantial contributions to the conception of the work. All authors substantially contributed to acquisition, analysis or interpretation of data for the manuscript, revising and critically reviewing the manuscript for important intellectual content. All authors approved the final version of this manuscript and agree to be accountable for all aspects of the work in ensuring that questions related to the accuracy or integrity of any part of the work are appropriately investigated and resolved. Funding acquisition and resources were provided by N.O.S.C., P.M.M.M.V., M.C., and M.A.R.V. M.C. and M.A.R.V. contributed to supervision of the study.

ADDITIONAL INFORMATION

The online version of this article (<https://doi.org/10.1038/s41385-020-00371-6>) contains supplementary material, which is available to authorized users.

Competing interests: The authors declare no competing interests.

Publisher's note Springer Nature remains neutral with regard to jurisdictional claims in published maps and institutional affiliations.

REFERENCES

1. Semenza, G. L. Life with oxygen. *Science* **318**, 62–64 (2007).
2. Fratantonio, D., Cimino, F., Speciale, A. & Virgili, F. Need (more than) two to Tango: multiple tools to adapt to changes in oxygen availability. *Biofactors* **44**, 207–218 (2018).
3. Lopez-Barneo, J., Pardo, R. & Ortega-Sáenz, P. Cellular mechanism of oxygen sensing. *Annu. Rev. Physiol.* **63**, 259–287 (2001).
4. Albenberg, L. et al. Correlation between intraluminal oxygen gradient and radial partitioning of intestinal microbiota. *Gastroenterology* **147**, 1055–1063.e1058 (2014).
5. Glover, L. E., Lee, J. S. & Colgan, S. P. Oxygen metabolism and barrier regulation in the intestinal mucosa. *J. Clin. Investig.* **126**, 3680–3688 (2016).

6. Fachi, J. L. et al. Butyrate protects mice from clostridium difficile-induced colitis through an HIF-1 α -dependent mechanism. *Cell Rep.* **27**, 750–761.e757 (2019).
7. Kelly, C. J. et al. Crosstalk between microbiota-derived short-chain fatty acids and intestinal epithelial hif augments tissue barrier function. *Cell Host Microbe* **17**, 662–671 (2015).
8. Masoud, G. N. & Li, W. HIF-1 α pathway: role, regulation and intervention for cancer therapy. *Acta Pharm. Sin. B* **5**, 378–389 (2015).
9. Semenza, G. L. Hydroxylation of HIF-1: oxygen sensing at the molecular level. *Physiology* **19**, 176–182 (2004).
10. Dengler, V. L., Galbraith, M. & Espinosa, J. M. Transcriptional regulation by hypoxia inducible factors. *Crit. Rev. Biochem. Mol. Biol.* **49**, 1–15 (2014).
11. Jain, I. H. et al. Genetic screen for cell fitness in high or low oxygen highlights mitochondrial and lipid metabolism. *Cell* **181**, 716–727.e711 (2020).
12. Wenger, R. H., Stiehl, D. P. & Camenisch, G. Integration of oxygen signaling at the consensus HRE. *Sci. STKE* **2005**, re12 (2005).
13. Vivier, E. et al. Innate lymphoid cells: 10 years on. *Cell* **174**, 1054–1066 (2018).
14. Longman, R. S. et al. CX₃CR1⁺ mononuclear phagocytes support colitis-associated innate lymphoid cell production of IL-22. *J. Exp. Med.* **211**, 1571–1583 (2014).
15. Wolk, K. et al. IL-22 increases the innate immunity of tissues. *Immunity* **21**, 241–254 (2004).
16. Cella, M. et al. A human natural killer cell subset provides an innate source of IL-22 for mucosal immunity. *Nature* **457**, 722–725 (2009).
17. Abt, M. C. et al. Innate immune defenses mediated by two ILC subsets are critical for protection against acute clostridium difficile infection. *Cell Host Microbe* **18**, 27–37 (2015).
18. Song, C. et al. Unique and redundant functions of NKp46+ ILC3s in models of intestinal inflammation. *J. Exp. Med.* **212**, 1869–1882 (2015).
19. Bando, J. K. et al. The tumor necrosis factor superfamily member RANKL suppresses effector cytokine production in group 3 innate lymphoid cells. *Immunity* **48**, 1208–1219.e1204 (2018).
20. Di Luccia, B., Gilfillan, S., Cella, M., Colonna, M. & Huang, S. C. ILC3s integrate glycolysis and mitochondrial production of reactive oxygen species to fulfill activation demands. *J. Exp. Med.* **216**, 2231–2241 (2019).
21. Fachi, J. L. et al. Acetate coordinates neutrophil and ILC3 responses against *C. difficile* through FFAR2. *J. Exp. Med.* **217**, jem.20190489 (2020).
22. Dang, E. V. et al. Control of T(H)17/T(reg) balance by hypoxia-inducible factor 1. *Cell* **146**, 772–784 (2011).
23. Wiperman, M. F., Montrose, D. C., Gotto, A. M. & Hajjar, D. P. Mammalian target of rapamycin: a metabolic rheostat for regulating adipose tissue function and cardiovascular health. *Am. J. Pathol.* **189**, 492–501 (2019).
24. Nagao-Kitamoto, H. et al. Interleukin-22-mediated host glycosylation prevents Clostridioides difficile infection by modulating the metabolic activity of the gut microbiota. *Nat. Med.* **26**, 608–617 (2020).
25. Krzywinska, E. & Stockmann, C. Hypoxia, metabolism and immune cell function. *Biomedicines*. **6**, 56 (2018).
26. Westendorf, A. M. et al. Hypoxia enhances immunosuppression by inhibiting CD4+ effector T cell function and promoting Treg activity. *Cell Physiol. Biochem.* **41**, 1271–1284 (2017).
27. Clambey, E. T. et al. Hypoxia-inducible factor-1 α -dependent induction of FoxP3 drives regulatory T-cell abundance and function during inflammatory hypoxia of the mucosa. *Proc. Natl Acad. Sci. USA* **109**, E2784–E2793 (2012).
28. Shi, L. Z. et al. HIF1 α -dependent glycolytic pathway orchestrates a metabolic checkpoint for the differentiation of TH17 and Treg cells. *J. Exp. Med.* **208**, 1367–1376 (2011).
29. Finlay, D. K. et al. PDK1 regulation of mTOR and hypoxia-inducible factor 1 integrate metabolism and migration of CD8+ T cells. *J. Exp. Med.* **209**, 2441–2453 (2012).
30. Sukumar, M. et al. Inhibiting glycolytic metabolism enhances CD8+ T cell memory and antitumor function. *J. Clin. Investig.* **123**, 4479–4488 (2013).
31. Krzywinska, E. et al. Loss of HIF-1 α in natural killer cells inhibits tumour growth by stimulating non-productive angiogenesis. *Nat. Commun.* **8**, 1597 (2017).
32. Li, Q. et al. E3 ligase VHL promotes group 2 innate lymphoid cell maturation and function via glycolysis inhibition and induction of interleukin-33 receptor. *Immunity* **48**, 258–270.e255 (2018).
33. Chang, C. H. et al. Posttranscriptional control of T cell effector function by aerobic glycolysis. *Cell* **153**, 1239–1251 (2013).
34. Pearce, E. L., Poffenberger, M. C., Chang, C. H. & Jones, R. G. Fueling immunity: insights into metabolism and lymphocyte function. *Science* **342**, 1242454 (2013).
35. Gerriets, V. A. et al. Foxp3 and Toll-like receptor signaling balance T. *Nat. Immunol.* **17**, 1459–1466 (2016).
36. Velásquez, S. Y. et al. Short term hypoxia synergizes with interleukin 15 priming in driving glycolytic gene transcription and supports human natural killer cell activities. *J. Biol. Chem.* **291**, 12960–12977 (2016).
37. Abt, M. C., McKenney, P. T. & Pamer, E. G. Clostridium difficile colitis: pathogenesis and host defence. *Nat. Rev. Microbiol.* **14**, 609–620 (2016).

38. Zheng, L., Kelly, C. J. & Colgan, S. P. Physiologic hypoxia and oxygen homeostasis in the healthy intestine. A review in the theme: cellular responses to hypoxia. *Am. J. Physiol. Cell Physiol.* **309**, C350–C360 (2015).
39. Jalili-Firoozinezhad, S. et al. A complex human gut microbiome cultured in an anaerobic intestine-on-a-chip. *Nat. Biomed. Eng.* **3**, 520–531 (2019).
40. Lin, N. & Simon, M. C. Hypoxia-inducible factors: key regulators of myeloid cells during inflammation. *J. Clin. Invest.* **126**, 3661–3671 (2016).
41. Higashiyama, M. et al. HIF-1 in T cells ameliorated dextran sodium sulfate-induced murine colitis. *J. Leukoc. Biol.* **91**, 901–909 (2012).
42. Gury-BenAri, M. et al. The spectrum and regulatory landscape of intestinal innate lymphoid cells are shaped by the microbiome. *Cell* **166**, 1231–1246.e1213 (2016).
43. Vonarbourg, C. et al. Regulated expression of nuclear receptor ROR γ t confers distinct functional fates to NK cell receptor-expressing ROR γ t(+) innate lymphocytes. *Immunity* **33**, 736–751 (2010).
44. Klose, C. S. et al. A T-bet gradient controls the fate and function of CCR6-ROR γ t+ innate lymphoid cells. *Nature* **494**, 261–265 (2013).
45. Rankin, L. C. et al. The transcription factor T-bet is essential for the development of NKp46+ innate lymphocytes via the Notch pathway. *Nat. Immunol.* **14**, 389–395 (2013).
46. Allan, D. S. et al. An in vitro model of innate lymphoid cell function and differentiation. *Mucosal Immunol.* **8**, 340–351 (2015).
47. Rempel, L. C. T. et al. Chronic exposure to hypoxia attenuates renal injury and innate immunity activation in the remnant kidney model. *Am. J. Physiol. Ren. Physiol.* **317**, F1285–F1292 (2019).
48. Chen, X. et al. A mouse model of Clostridium difficile-associated disease. *Gastroenterology* **135**, 1984–1992 (2008).
49. Monteiro, L. B., Davanzo, G. G., de Aguiar, C. F. & Moraes-Vieira, P. M. M. Using flow cytometry for mitochondrial assays. *MethodsX* **7**, 100938 (2020).



Open Access This article is licensed under a Creative Commons Attribution 4.0 International License, which permits use, sharing, adaptation, distribution and reproduction in any medium or format, as long as you give appropriate credit to the original author(s) and the source, provide a link to the Creative Commons license, and indicate if changes were made. The images or other third party material in this article are included in the article's Creative Commons license, unless indicated otherwise in a credit line to the material. If material is not included in the article's Creative Commons license and your intended use is not permitted by statutory regulation or exceeds the permitted use, you will need to obtain permission directly from the copyright holder. To view a copy of this license, visit <http://creativecommons.org/licenses/by/4.0/>.

© The Author(s) 2021

